JGR Planets

RESEARCH ARTICLE

10.1029/2025JE009458

Present-Day Thermal State and Surface Heat Flux of the Moon

Sabatino Santangelo[1], **Ana-Catalina Plesa**[1], **Adrien Broquet**[1], **Doris Breuer**[1], and **Matthias Grott**[1]

[1]German Aerospace Center (DLR), Institute of Space Research, Berlin, Germany

Key Points:

- We model the thermal evolution of the Moon and constrain the distribution of interior heat sources using Apollo heat flux measurements
- A unit with an average thickness of 1.6 km, 1,200–1,600 km radius, and 23–50 ppm Th at the base of the crust matches best the heat flux data
- Models predict a surface heat flux of 7–12 and 8–14 mW/m^2 for upcoming measurements at Mare Crisium and Schrödinger basin, respectively

Supporting Information:

Supporting Information may be found in the online version of this article.

Correspondence to:

S. Santangelo,
Sabatino.Santangelo@dlr.de

Citation:

Santangelo, S., Plesa, A.-C., Broquet, A., Breuer, D., & Grott, M. (2025). Present-day thermal state and surface heat flux of the Moon. *Journal of Geophysical Research: Planets*, *130*, e2025JE009458. https://doi.org/10.1029/2025JE009458

Received 24 SEP 2025
Accepted 21 NOV 2025

Author Contributions:

Conceptualization: Sabatino Santangelo, Ana-Catalina Plesa, Adrien Broquet, Doris Breuer, Matthias Grott
Formal analysis: Sabatino Santangelo
Funding acquisition: Ana-Catalina Plesa, Doris Breuer
Investigation: Sabatino Santangelo
Methodology: Sabatino Santangelo, Ana-Catalina Plesa, Adrien Broquet
Project administration: Ana-Catalina Plesa
Software: Sabatino Santangelo, Ana-Catalina Plesa
Supervision: Ana-Catalina Plesa, Adrien Broquet, Doris Breuer
Validation: Sabatino Santangelo
Visualization: Sabatino Santangelo

Abstract The concentration of volcanic material and Heat-Producing Elements (HPE) on the lunar nearside surface suggests an asymmetry of interior properties and thermal history between the two hemispheres. However, the distribution of HPE beneath the surface and the processes that led to their potential enrichment on the nearside remain poorly understood. Here, we use a 3D geodynamic model to infer the interior distribution of HPE based on surface heat flux estimates. We explore the consequences of a putative HPE-rich unit underneath the Procellarum region on the lateral variations of the present-day surface heat flux. Assuming a circular geometry and 1.6 km average thickness, we explore various sizes, locations, and enrichments of the HPE-rich unit, including the complete absence of such an anomaly, and select successful scenarios based on models that match the Apollo heat flux measurements. Scenarios with either a homogeneous HPE distribution in the mantle or a globally uniform HPE-rich layer lead to surface heat fluxes inconsistent with Apollo data. Conversely, a HPE anomaly beneath the nearside, extending at least to the Apollo 15 landing site and at most encircling the entire mare region, including Apollo 17 landing site, can match both measurements. The required Th concentration within the anomaly ranges from 23 to 50 ppm, assuming a 1.6 km thickness. Finally, we predict heat flux ranges of 7–12 mW/m^2 and 8–14 mW/m^2 for the upcoming Blue Ghost Mission 1 and APEX®1.0 heat flux measurements.

Plain Language Summary The Moon shows striking differences between its near- and farside surface: most volcanic material and heat sources (such as uranium and thorium) are found on the side facing Earth. Such uneven distribution suggests a different interior beneath the two hemispheres, but the origin and deeper structure of this difference remain unclear. In this study, we investigate the thermal history of the Moon in order to explore how the distribution of heat sources affects the heat loss through the lunar surface. We focus on the surface region called the Procellarum KREEP Terrane (PKT), known for its high concentrations of heat sources. We model a subsurface layer rich in heat sources beneath this region and vary the layer's heat sources, size, and position. Model results are then compared with available heat flux data. We find that globally uniform distributions of heat sources are inconsistent with the measured Apollo heat fluxes. The same holds for a radiogenic anomaly that does not extend at least beneath Apollo 15 landing location. Instead, the presence of a large-scale subsurface anomaly in heat sources is required to match the available constraints. Finally, we predict heat flow values to be measured by upcoming missions, and discuss their implications.

1. Introduction

Since the first image of the Moon's farside was taken by soviet Luna 3 spacecraft in 1959, multiple data sets have revealed a striking asymmetry between the nearside Procellarum KREEP (Potassium, Rare-Earth Elements, and Phosphorus) Terrane (PKT; Jolliff et al., 2000) and the surrounding feldspathic highlands. Among other data sets, the asymmetry spans volcanic history, surface gravity, topography, and surface composition (e.g., Broquet & Andrews-Hanna, 2024b; Hiesinger et al., 2023; Lawrence et al., 1999; Smith et al., 2010; Zuber et al., 2013). Notably, the PKT region is characterized by its elevated surface concentrations of Th, implying corresponding enhancements in other Heat Producing Elements (HPE; U, Th, K) through characteristic abundance ratios (S. Taylor, 1982). Furthermore, the surface Th anomalies are believed to correlate with ejecta deposited by the Imbrium impact, indicating that a subsurface HPE-rich reservoir potentially existed beneath Mare Imbrium at the time of its formation (Haskin, 1998). This evidence is of crucial importance, as a HPE enrichment in the nearside subsurface could have kept the mantle warmer throughout the evolution of the Moon, potentially explaining the long-lasting volcanic activity in the region (Hiesinger et al., 2023; Laneuville et al., 2013; Wieczorek &

Writing – original draft: Sabatino Santangelo
Writing – review & editing: Sabatino Santangelo, Ana-Catalina Plesa, Adrien Broquet, Doris Breuer, Matthias Grott

Phillips, 2000). However, the HPE concentration, lateral extent and thickness of the subsurface reservoir remain poorly constrained.

Measurements of surface heat flux (or heat flow density, expressed in W/m^2) are sensitive to the concentration of HPE beneath the surface, offering a way to probe the distribution of heat sources within the planetary interior. On the Moon, the Apollo 15 and 17 missions measured local surface heat flux values of 21 ± 3 and 14 ± 2 mW/m^2 at 26°N–3.6°E and 20°N–30.8°E, respectively (Langseth et al., 1976). The two Apollo measurements were later corrected down to 18 ± 3 and 12 ± 2 mW/m^2 to better represent regional values, accounting for lateral heat flow focusing within thin-crust basins (Warren & Rasmussen, 1987). The heat flow focusing effect at the boundary between maria and highlands has also been confirmed using high-resolution topography and crustal thickness in Siegler and Smrekar (2014). We note that the revised values (18 ± 3 and 12 ± 2 mW/m^2) should be used when the heat flow focusing effect is neglected or not resolved; otherwise, the original measurements (21 ± 3 and 14 ± 2 mW/m^2) should be used, for example, when lateral variations in crustal thickness or crustal thermophysical properties are considered.

More recently, remote sensing estimates reported low heat flux values of 5–6 mW/m^2 in permanently shadowed regions near the lunar south pole (Paige & Siegler, 2016; Wei et al., 2023), hereafter referred to as Region 5 estimate, and up to 180 mW/m^2 at the Compton–Belkovich Th anomaly, near the north pole (Siegler et al., 2023). These remote-sensing estimates come from geologically unusual sites (a permanently shadowed crater and the strongest isolated Th anomaly) and lack uncertainty quantification, making them harder to interpret than in situ measurements. In summary, the limited number and spatial bias of heat flux data (i.e., lack of any farside data) complicate the interpretation of lunar interior and HPE distribution models.

Nevertheless, previous studies successfully used global thermo-chemical evolution models to find subsurface HPE distributions that could explain Apollo heat flux data as well as other geophysical constraints (Laneuville et al., 2013, 2018). Notably, modeling results from Laneuville et al. (2013) suggest that the Moon's prolonged volcanic activity is best explained by an HPE-rich layer located between crust and mantle, and that the most recent magmatic events occur in the center of the anomaly. Moreover, the models in Laneuville et al. (2018) show that the Apollo 15 and 17 measurements, along with the Region 5 estimate, are consistent with a cylindrical subsurface HPE-rich unit of ∼1,300 km in radius, 26.4 km thickness, and enriched in Th by ∼5.7 ppm.

These thickness values for the subsurface HPE anomaly seem to be in conflict with the results of magma ocean crystallization models (e.g., Schwinger & Breuer, 2022), which predict a much thinner unit (<2 km). This thin HPE anomaly predicted by magma ocean crystallization models is representative of the so-called urKREEP layer that is sandwiched between the anorthositic crust and the Ilmenite Bearing Cumulate (IBC) layer (as defined in Warren & Wasson, 1979). It is uncertain whether this urKREEP layer still exists in this form or has been mixed with upper mantle melt and formed a thicker layer of KREEP basalt, which is then less enriched in radiogenic heat sources, and has been suggested to be present today underneath the PKT region (Laneuville et al., 2013; Wieczorek & Phillips, 2000). In addition, global models are tipically limited in radial resolution and are forced to dilute the HPE enrichments in much thicker layers (e.g., a 26.4 km-thick layer of 5.7 ppm Th concentration is equivalent to a 2 km-thick layer of ∼75 ppm Th concentration).

Furthermore, in both Laneuville et al. (2013, 2018), all model parameters, including crustal thickness, are laterally uniform except for the presence of the HPE anomaly. As a result, the geodynamic models lack a specific orientation, and surface locations such as Apollo 15 and 17 landing sites cannot be uniquely identified beyond their radial distance from the anomaly center. The absence of an orientation limits the ability to correlate model results with other geophysical evidence, such as the distribution and age of mare basalts (Hiesinger et al., 2023).

Regional models can incorporate lateral variations in topography, crustal thickness, and heat sources distribution, enabling precise localization of the heat flux measurements (e.g., Siegler & Smrekar, 2014). Their scope, however, is restricted to limited surface areas and shallow depths (e.g., 1,500 × 2,700 km laterally and 150 km deep in Siegler & Smrekar, 2014) and relies on assumptions about mantle contributions to surface heat flux. These limitations hinder the ability to derive implications from regional results to global scales.

Lastly, recent studies have further constrained key parameters for thermal evolution modeling, including the mineralogical composition of the lunar interior (Haupt et al., 2024; Schwinger & Breuer, 2022), and the Th content of the HPE reservoir excavated by the Imbrium impact (Levin et al., 2025). These advances highlight the

need for a new generation of global thermal evolution models that can combine lateral variability with an updated interior structure, informed by recent petrological and geophysical evidence, as mentioned in Siegler and Smrekar (2014), Gaffney et al. (2023), and Andrews-Hanna et al. (2023).

In this work, we expand on the work in Laneuville et al. (2013, 2018), and obtain new constraints on the Moon's interior HPE distribution. Our model includes both spatial variability in crustal thickness and a more complex geometry for the Th source unit. We note that this work does not aim to model the processes that may have caused these lateral variations, but rather investigate their effect on the present-day thermal state of the Moon. Using this model setup, we perform an extensive parameter exploration based on the constraints on Th source enrichment, subsurface structure and bulk HPE abundance proposed by Levin et al. (2025), Schwinger and Breuer (2022), Haupt et al. (2024), and G. Taylor and Wieczorek (2014).

Moreover, our models can be used to better interpret regional models and upcoming in situ measurements. For instance, Firefly's Blue Ghost Mission 1 (recently landed in Mare Crisium on 02/03/2025), and Ispace's APEX®1.0 (scheduled to land in Schrödinger crater in 2026) are both equipped with a heat flux probe and will soon provide new in situ heat flux measurements at key locations on the lunar surface. Our best-fit models provide testable hypotheses on the surface heat flux and subsurface thermal state at any time and location on the Moon, including these landing sites, with strong implications for the distribution of HPE and the structure of the lunar interior. In the following sections, we review the measurements relevant to this study (Section 2), describe our methods (Section 3), present our main findings (Section 4), and finally discuss their implications for the evolution of the Moon (Section 5).

2. Heat Flux Measurements and Uncertainties

Caution is required when comparing heat flux results from global geodynamical models to the Apollo heat flux data, as the reported values depend on corrections that were applied to the data. In situ surface heat flux measurements from Apollo 15 and 17, corrected for local topographic and subsurface effects, were reported by Langseth et al. (1976), with values of 21 and 14 mW/m^2, respectively. The associated uncertainties reported by Langseth et al. (1976) are equal to ±15% (i.e., ±3.15 mW/m^2 for Apollo 15 and ±2.1 mW/m^2 for Apollo 17), and are primarily due to uncertainties in the estimation of thermal diffusivity. The Apollo measurements were later revised to account for heat flow focusing at the maria–highlands boundary, which may increase surface heat flux locally at the Apollo 15 and 17 sites by 10–15% relative to the maria average and by 20–40% relative to the highlands average (Grott et al., 2010; Warren & Rasmussen, 1987). This effect is caused by the lower bulk thermal conductivity, thicker crust and thicker megaregolith layer above the anorthositic highlands, which provide better insulation and favor lateral heat flow towards the maria where heat can more easily escape.

Remote sensing estimates of surface heat flux have been reported for the south polar regions (i.e., 5–6 mW/m^2; Paige & Siegler, 2016; Wei et al., 2023) and the Compton–Belkovich region (i.e., ∼180 mW/m^2; Siegler et al., 2023), but without associated uncertainties. The absence of error bars, combined with the large difference between these estimates, makes them inherently less reliable than in situ measurements. Uncertainties in remote estimates, particularly at low flux values, mainly arise from poorly constrained parameters such as regolith thermophysical properties and subsurface water abundance in permanently shadowed regions. Given these uncertainties, and in particular those related to the water content in the subsurface, we cannot exclude heat flux values as high as 12–14 mW/m^2 at the south pole, which prevents us from using these estimates as direct constraints.

3. Methods

3.1. Mantle Convection

We simulate the thermal evolution of the Moon using the mantle convection code GAIA-v2 (Hüttig & Stemmer, 2008a; Hüttig et al., 2013) in a 3D spherical geometry (Hüttig & Stemmer, 2008b; Plesa, Hüttig, et al., 2016). We use a structured grid with 91 radial layers, with 8 km resolution from the surface to 76 km depth, and 16 km resolution from 76 km depth to the core–mantle boundary (i.e., 1,350 km depth). Each layer contains 40,962 cells laterally, corresponding to ∼15 × 15 km resolution at mid-mantle depth and ∼30 × 30 km resolution at the surface, for a total of ∼3.73 million grid points for each simulation. Increasing the grid size to 5.8 million points, with 4 km radial resolution from the surface to 76 km depth, and 10.5 km resolution from 76 km depth to the core–

Table 1
Parameters Used for Initializing the Thermal Evolution Model

Symbol	Description	Value	Unit
R_p	Planet radius	1,740	km
R_c	Core radius	390	km
D	Mantle thickness (R_p - R_c)	1,350	km
D_i	Dissipation number	0.04374	[-]
E	Activation energy	3×10^5	J mol^{-1}
R	Universal gas constant	8.314	J mol^{-1} K^{-1}
T_0	Surface temperature	250	K
T_c	Initial core temperature	2,000	K
T_r	Reference temperature	1,600	K
ΔT	Temperature variation in the mantle	1,750	K
Th/U	Thorium to uranium ratio	3.7	[-]
K/U	Potassium to uranium ratio	2,500	[-]
V	Activation volume	6×10^{-6}	m^3
c_p	Mantle specific heat capacity	1,000	J kg^{-1} K^{-1}
$c_{p,\mathrm{core}}$	Core specific heat capacity	800	J kg^{-1} K^{-1}
g	Surface gravity acceleration	1.62	m s^{-2}
k_c	Crust thermal conductivity	1.5	W m^{-1} K^{-1}
k_K	KREEP unit thermal conductivity	1.5	W m^{-1} K^{-1}
k_r	Reference thermal conductivity (mantle)	3	W m^{-1} K^{-1}
p_r	Reference pressure	3	GPa
z_r	Reference depth	545	km
α_r	Reference thermal expansivity	2×10^{-5}	K^{-1}
η_r	Reference viscosity	10^{21}	Pa s
κ_r	Reference thermal diffusivity	8.82×10^{-7}	m^2 s^{-1}
ρ_r	Reference density (mantle)	3,400	kg m^{-3}
ρ_c	Crustal density	2,500	kg m^{-3}
ρ_K	KREEP unit density	2,500	kg m^{-3}
ρ_{core}	Core density	7,400	kg m^{-3}

Note. Most parameters are taken from Laneuville et al. (2013) and references therein. The rheological parameters (i.e., E and V) are taken from Karato and Wu (1993). The Th/U and K/U ratios are taken from S. Taylor (1982).

mantle boundary yielded negligibly different results (Section S1.1 in Supporting Information S1), at the expense of a higher computational cost.

Each model consists of a mantle overlain by a crust (average thickness ~40 km; Broquet & Andrews-Hanna, 2024a; Wieczorek et al., 2013), and a thin HPE–rich unit (average thickness ~8 km, limited by model resolution) located between them. In themselves, all three layers are compositionally homogeneous and characterized by the parameters listed in Table 1. The concentration of HPE (i.e., ^{238}U, ^{235}U, ^{232}Th, and ^{40}K) varies between the layers, and we account for the time-dependent internal heating due to their radioactive decay (see Section S1.2 in Supporting Information S1 for the governing equations). Hereafter, we will use Th as a proxy for HPE, assuming that the radiogenic elements are always related by constant Th/U and K/U ratios of 3.7 and 2,500, respectively (S. Taylor, 1982).

The thermal evolution simulations start after the crystallization of the Lunar Magma Ocean (LMO) and proceed until present day (~4.5 Gyr). From the resulting present-day thermal state, we calculate the surface heat flux distribution (as a 2D map) and compare it with Apollo measurements, Region 5, and Compton-Belkovich

estimates. For each HPE distribution tested, we simulate the full thermal evolution to avoid imposing assumptions on the present-day mantle heat flux contribution, which can reach ∼7–9 ± 1.5 mW/m^2. Core cooling is implemented as a one-dimensional, time-dependent boundary condition at the core–mantle boundary, following Steinbach and Yuen (1994) and Stevenson et al. (1983). Core dynamics, crystallization, and inner core growth are not included in the model.

Finally, the mantle temperature in our model is initialized using the same method and intermediate initial temperature profile of Laneuville et al. (2013). Furthermore, we tested the "hot" and "cold" profiles (variations of ±200 K in the initial temperature), which imply variations in viscosity and convection vigor during the early evolution. As expected, the mentioned variations have negligible effects on the present-day surface heat flux at the Apollo 15 and 17 landing sites (<1 mW/m^2). We note that any initial temperature and viscosity conditions, while important for the early evolution, will have a negligible effect on the present-day thermal state and surface heat flux. This is due to the so-called "thermostat effect" in planetary mantles (Schubert et al., 1979).

3.2. Constant Crust and HPE-Rich Unit Thickness Setup

In the first part of this study, we adopt a simplified model setup with a laterally uniform crustal thickness and HPE-rich unit thickness (40 and 8 km, respectively). This configuration is directly comparable to previous thermo-chemical evolution models (Laneuville et al., 2013, 2018) and LMO crystallization studies (e.g., Schwinger & Breuer, 2022), making it well-suited for a first-order investigation of the lateral extent and enrichment of a subsurface HPE anomaly. We test four initial configurations for a HPE-rich unit sandwiched between crust and mantle. These are termed global, hemispherical, regional, and absent, respectively. In the hemispherical and regional cases, the subsurface HPE anomaly is modeled as a cylindrical cap of radius ∼2,700 km and ∼1,300 km, respectively, due to the lack of constraints on its shape. For each simulation, we compare the present-day surface heat flux distribution with the Apollo measurements, focusing on whether the modeled anomaly can reproduce values as high as the maximum observed (Apollo 15). For this simplified setup, we must compare the modeled heat flux with the revised Apollo values (18 ± 3 mW/m^2, 12 ± 2 mW/m^2), since this model does not account for any heat flow focusing effects (Warren & Rasmussen, 1987).

In terms of HPE distribution, we keep the bulk silicate Moon and crustal concentrations constant throughout this analysis. We assume Earth-like bulk silicate Moon abundances of 0.075 ppm Th following G. Taylor and Wieczorek (2014), and references therein. Crustal concentrations are assumed equal to 0.4 ppm Th, which is chosen as an intermediate value between the 0.05 and 0.8 ppm Th end-members obtained from sample analysis and surface composition studies (Meyer, 2004; Jolliff et al., 2000, respectively).

First, we model a globally uniform HPE-rich layer trapped between mantle and crust, representing the outcome of a perfectly symmetrical LMO crystallization. We refer to the global HPE-rich layer as urKREEP (defined in Warren & Wasson, 1979). The concentration of HPE in the urKREEP layer is constrained by an LMO fractional crystallization model that includes the equilibrium partition equation from Longhi (1980) and new Th partition coefficients for feldspar and pigeonite from experiment GPC866 in Haupt et al. (2024). The full set of parameters can be found in Supporting Information S1 (Section S1.3). This approach predicts concentrations of ∼18.7 ppm Th and a thickness of 1.6 km for the urKREEP layer, consistent with the estimates in Warren and Wasson (1979). In our geodynamical model, due to the limited radial resolution of our setup (Section 3.1), the HPE are diluted in an 8 km-thick layer, resulting in an equivalent concentration of 3.74 ppm Th.

Second, we model a scenario in which 100% of the urKREEP material overturns and homogeneously remixes into the mantle, resulting in a concentration of ∼0.055 ppm Th. Then, we investigate scenarios of urKREEP material sequestration into a hemispherical or regional subsurface unit, varying between 0% and 100% of the urKREEP material being concentrated in the unit. An example sketch of our simplified model setup, in case of a regional HPE anomaly and 50% urKREEP material sequestration, is provided in Figure 1. For all scenarios, we compare the present-day surface heat flux values with the revised Apollo measurements (18 ± 3 and 12 ± 2 mW/m^2 for Apollo 15 and 17, respectively).

3.3. Laterally Variable Crust and HPE-Rich Unit Thickness Setup

In the second part of this study, we investigate local variations in present-day surface heat flux at the Apollo 15, Apollo 17, and Region 5 sites by introducing lateral variations in crust and HPE-rich layer thicknesses, similar to

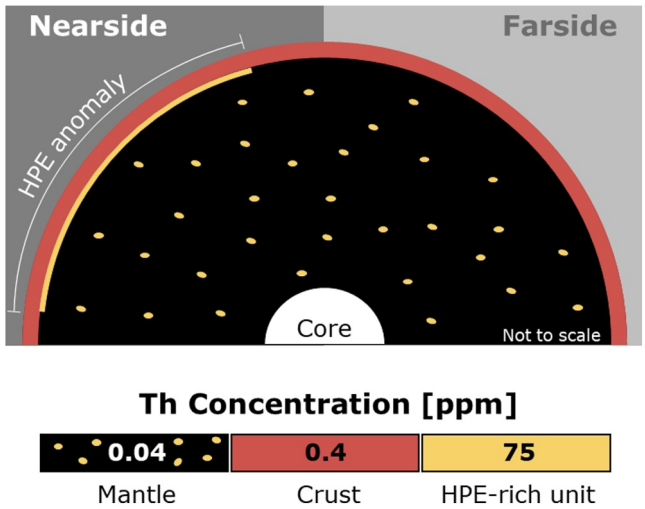

Figure 1. Schematic sketch of an example 3D model setup with constant crustal thickness and HPE-rich unit thickness. The three reservoirs (mantle, HPE-rich unit, and crust) differ in HPE concentration, which is represented by the color scheme. The HPE-rich unit is modeled as a circular cap, equivalent to a unit of 1.6 km thickness and ~75 ppm Th concentration. The mantle and the crust have Th concentrations of 0.04 and 0.4 ppm, respectively. Yellow dots are used to represent the percentage of HPE-rich material that is, remixed in the mantle and contribute to its heat production.

the approach by Plesa, Grott, et al. (2016). We take the crustal thickness distribution from the preferred model in Broquet and Andrews-Hanna (2024a), which fits observed gravity and topography data and considers the presence of the high-density mare units, re-plotted in Figure 2a. In this more sophisticated setup, the spatial variability in crustal thickness allows us to mimic the lateral heat flow within basins, as predicted in Warren and Rasmussen (1987). Thus, for these models, we compare our results with the original Apollo heat flux measurements (21 ± 3 mW/m^2, 14 ± 2 mW/m^2).

In addition, a laterally variable crustal thickness enables us to assess the effect of crustal thickness on surface heat flux distribution, uniquely identify surface locations, and track their subsurface thermal evolution over time. In our model, the present-day crustal structure is imposed at the start of the simulation, immediately after LMO crystallization. Although this approach neglects crustal modifications through impact events and volcanism, such early processes have limited effects on the surface heat flux at present day.

Our simulations consider a layer enriched in HPE at the base of the average crust of the maria region (i.e., ~32 km; Broquet & Andrews-Hanna, 2024a). In regions where the crust is thinner than this average, the HPE-rich unit is absent, and in regions of thicker crust, the HPE-rich unit will be thicker (always extending to the base of the crust). If present, the HPE-rich layer has a minimum thickness of 8 km, which represents our model radial resolution. This captures the effects of crustal thinning produced by large basins, which would have excavated the HPE-rich unit (e.g., Mare Imbrium and Serenitatis). Moreover, it mimics the effect of HPE-rich ejecta deposition by considering a thicker HPE-rich layer in regions of thicker crust surrounding basins such as Imbrium (Figure 2b).

Using the laterally variable model setup, we investigate all key parameters controlling surface heat flux: (a) concentration of radiogenics in the HPE-rich unit, (b) bulk silicate Moon HPE concentration, (c) lateral extent of the HPE-rich unit, and (d) crustal HPE concentration. The concentration in the HPE-rich unit is varied between 30 and 120 ppm Th, based on previous estimates for the Imbrium ejecta source region (Laneuville et al., 2013; Levin et al., 2025), with a lower end-member scenario of 14 ppm Th representing an Apollo 15 KREEP basalt Th concentration (Jolliff et al., 2000). As described in Section 3.2, concentrations in the HPE-rich unit are always expressed assuming a 1.6 km average layer thickness, and diluted in a thicker unit in our model (8 km on average) using a volume weighted equivalence.

For the bulk silicate Moon, we used concentrations in the Earth-like range of ~0.06–0.09 ppm Th (G. Taylor & Wieczorek, 2014, and references therein), as well as a testing a lower-end case of ~0.05 ppm Th, which is outside the proposed range and thus considered less likely. The radius of the HPE-rich unit is varied between ~800 and 2,700 km, and crustal HPE concentrations from ~0.1–0.8 ppm Th, based on lunar sample data analysis (e.g., Meyer, 2004) and surface Th observations (e.g., Jolliff et al., 2000).

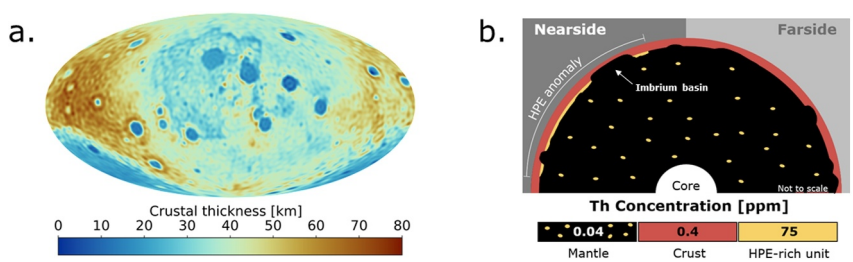

Figure 2. (a) Crustal thickness map based on GRAIL data (Broquet & Andrews-Hanna, 2024a), used in this study as input for global thermal evolution models considering lateral crustal thickness variations. (b) Sketch of the model setup including crustal thickness variations, using the same color code as in Figure 1. This more sophisticated model is characterized by a laterally variable crustal thickness (~40 km on average) and HPE-rich unit that is, located at the base of the crust.

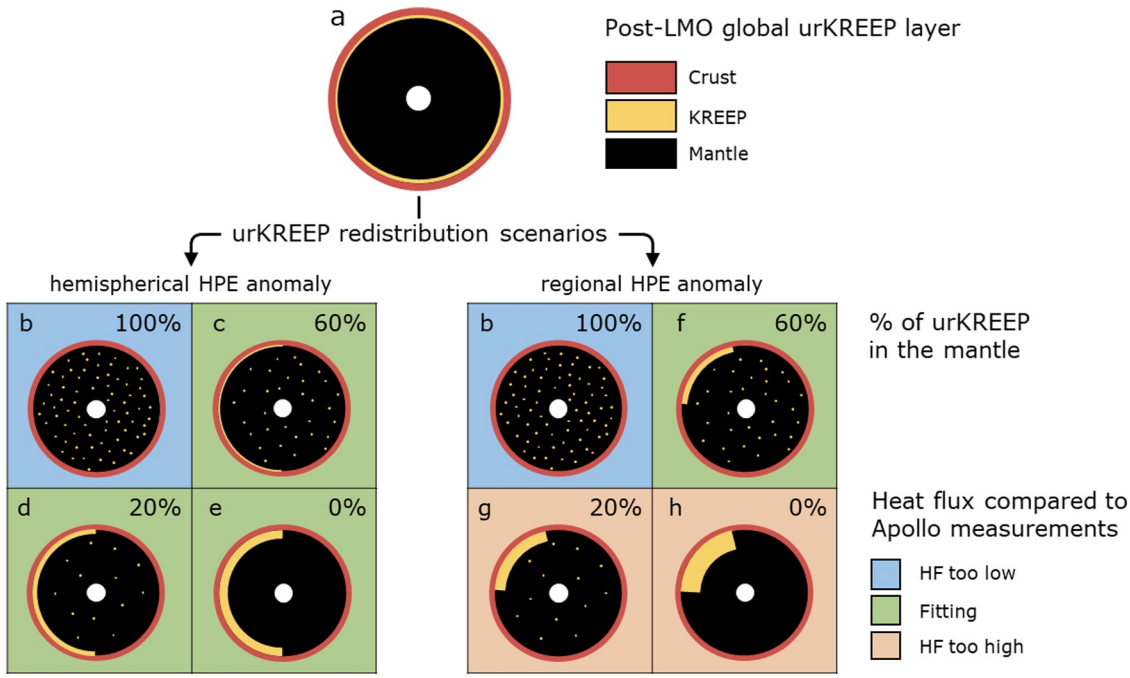

Figure 3. Summary of our tested scenarios using constant crustal thickness and HPE-rich unit thickness. Each cross-section represents a thermal evolution simulation with different HPE distribution. (a) Global urKREEP layer configuration resulting from symmetric LMO crystallization (∼18 ppm Th in the urKREEP, ∼0.02 ppm Th in the mantle). (b) Case of complete remixing of urKREEP into the mantle (∼50 ppm Th in the mantle). (c–e) Simulations with increasing concentration of HPE underneath the nearside crust, for a hemispherical unit (15, 30, and 35 ppm Th in the unit, respectively). (f–h) Analogous to (c)–(e), but for a regional nearside anomaly of ∼1,300 km radius (50, 100, 125 ppm Th for a 1.6 km-thick unit, respectively). Note: thickness of the layers in the figure is not to scale.

4. Results

4.1. Constraining the Extent of the HPE-Rich Unit

Using the constant thickness model (Section 3.2), we test four geometries for a subsurface HPE-rich unit: global, hemispherical, regional (i.e., ∼1,300 km radius), and absent (i.e., HPE are completely redistributed in the mantle). In addition, we vary the HPE enrichment of the regional and hemispherical units to investigate the degree of HPE sequestration needed to explain the Apollo measurements (Figure 3). We note that all models produce an average surface heat flux value of ∼12 mW/m^2 at present-day, consistent with the estimates in Warren and Rasmussen (1987). Depending on the model parameters, the mantle contribution to the surface heat flux is on average up to 7 − 9 mW/m^2 with variations of ±1.5 mW/m^2.

In case of a globally uniform urKREEP layer (Figure 3a) we find that present-day surface heat flux variations are negligible (within 0.3 mW/m^2), as expected. The average surface heat flux is equal to ∼12 mW/m^2 in this case, which is consistent with the Apollo 17 revised measurement (12 ± 2 mW/m^2), but too low for Apollo 15 (18 ± 3 mW/m^2). The configuration with a homogeneous remixing of HPE into the lunar mantle (Figure 3b) yields a similar surface heat flux distribution, everywhere equal to ∼12 mW/m^2. We note that the similarity between these two cases is expected, due to the spatial symmetry of both configurations. Since the predicted heat flux is too low to explain Apollo 15 measurement, we consider these two scenarios less likely ("HF too low" in Figure 3).

For configurations with a hemispherical anomaly (Figures 3c–3e), present-day surface heat flux values are consistent with Apollo measurements when 0%–60% of urKREEP material is mixed into the mantle. This scenario yields surface heat fluxes of ∼14–16 mW/m^2 above the HPE-rich region. These results suggest that a hemispherical HPE asymmetry could explain the elevated heat flux measured by Apollo, provided that the anomaly contains at least ∼15 ppm Th within a 1.6 km-thick layer (Figure 3c). We note that a trade-off between layer thickness and enrichment is always possible.

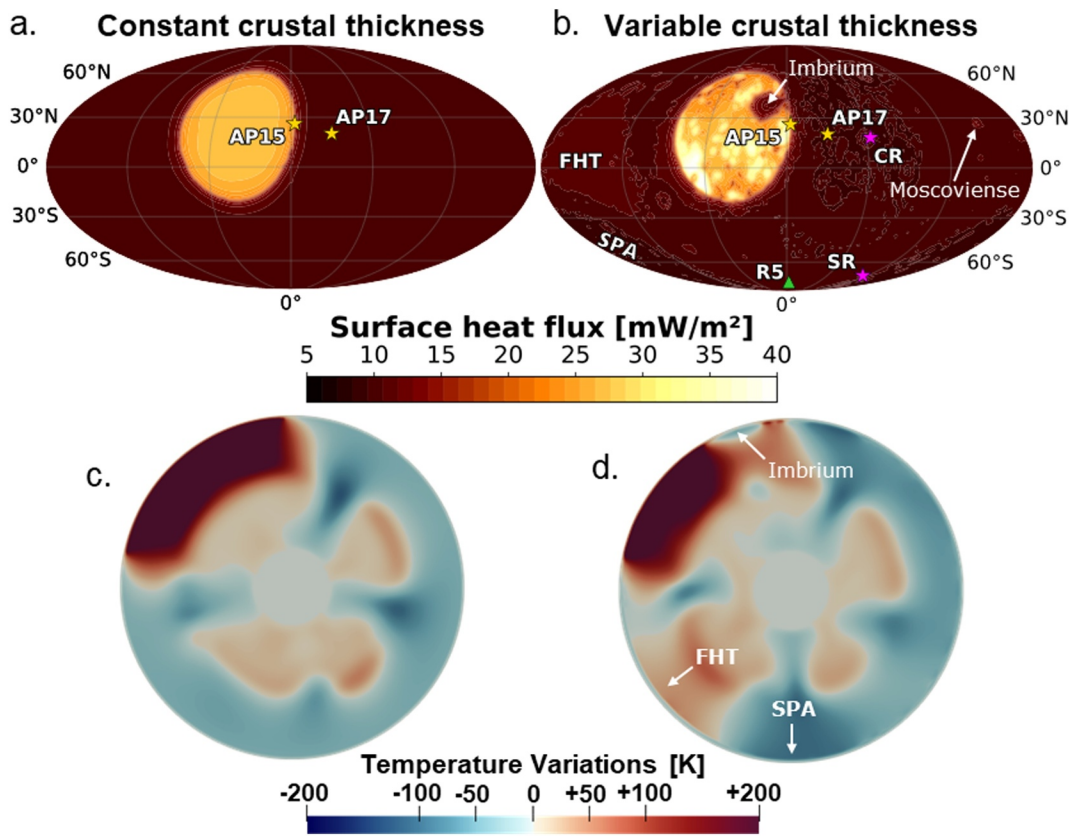

Figure 4. (a, b) Surface heat flux maps and (c, d) interior temperature variations at present day. Panels (a and c) show a model with a constant crustal thickness and HPE-rich unit thickness, while panels (b) and (d) show a scenario with a spatially variable crustal and HPE-rich unit thickness (i.e., 1,200 km HPE-rich unit radius, 0.075 ppm bulk Th concentration, 0.4 ppm crustal Th concentration, 75 ppm HPE-rich unit Th concentration). The symbols in the panels indicate the landing sites of Apollo 15 and Apollo 17 (AP15 and AP17), Region 5 (R5, south polar region), and future measurements locations (Mare Crisium—CR, Schrödinger Crater—SR). In addition, we indicate the Farside Highlands Terrane (FHT), South-Pole Aitken basin (SPA), Mare Imbrium, and Moscoviense. Note: panels (a) and (c) show results consistent with those in Laneuville et al. (2013). Panels (c) and (d) correspond to the great circles cutting through Imbrium, PKT, FHT, and SPA terrains.

In case of a regional anomaly (Figures 3f–3h), we find that surface heat flux values consistent with Apollo measurements require relatively weak HPE enrichments, from 60% of urKREEP material mixed into the mantle (Figure 3g) to an ~85% end-member case (not shown, intermediate case between Figures 3f and 3g). Conversely, when more than 40% of the urKREEP material is concentrated in the anomaly (i.e., <60% urKREEP left in the mantle), present-day surface heat flux values exceed 23 mW/m^2 within the PKT region, which is inconsistent with the Apollo 15 measurement.

4.2. Effect of Crustal Thickness Distribution on the Spatial Variations of the Surface Heat Flux

The spatial variations in crustal thickness introduce substantial heterogeneities in the present-day surface heat flux distribution (±5 mW/m^2, Figures 4a and 4b). The higher HPE concentration in the crust with respect to the mantle causes regions of thick crust to have more subsurface heat sources than regions of thin crust. For example, the thick-crust Farside Highlands Terrane (FHT) shows a higher surface heat flux than the South-Pole Aitken basin (SPA, Figure 4b), with the difference being proportional to the crustal HPE concentration. Additionally, because the thermal conductivity of the crust is half that of the mantle (Table 1), a thicker insulating layer prevents heat escape more efficiently than a thin layer, and this leads to a higher subsurface temperature beneath thick crustal regions (e.g., FHT) than thin-crust regions (e.g., SPA, Figures 4c and 4d).

In other words, including crustal thickness variations in the models changes the planform of convection throughout the thermal evolution (Figures 4c and 4d). Unlike the present-day convection planform of a laterally

constant model (Figure 4c), a variable crustal thickness induces thermal anomalies that can extend from the deep mantle to the crust-mantle interface (Figure 4d). In particular, a positive and deeply rooted thermal anomaly induced by the thick-crust farside highlands (FHT) is visible in Figure 4d to the bottom left, whereas a negative anomaly corresponding to the crustal thinning in SPA can be seen on the bottom part of the same figure.

As mentioned in Section 3.2, we assume a bulk crustal enrichment of 0.4 ppm Th, which is an intermediate value between the concentration observed in anorthositic samples and that measured by surface gamma-ray spectrometry (Jolliff et al., 2000; Meyer, 2004). Using 0.4 ppm Th, the crustal thickness variations alone lead to a maximum difference in heat flux between lowlands (e.g., South-Pole Aitken, thin crust basins) and farside highlands of ∼3 mW/m^2 (Figure 4b). This value increases to ∼6 mW/m^2 for a crustal enrichment of 0.8 ppm Th, and decreases to ∼1 mW/m^2 for a crustal enrichment of 0.1 ppm Th (the corresponding surface heat flux maps are shown in the additional information Section S2.1 in Supporting Information S1).

Furthermore, lateral variability in the thickness of the HPE-rich unit has significant effects on both the surface heat flux and the interior temperature distribution (Figures 4b and 4d). The maximum difference between the heat flux within the HPE-rich region and a location of identical crustal thickness outside of the region is ∼30 mW/m^2. Although we consider a simplified circular geometry for the HPE-rich unit, our treatment of the unit thickness simulates the effect of basin excavation and thick ejecta deposition (Figure 4b), with a local minimum in surface heat flux corresponding to the center of Mare Imbrium and several local maxima surrounding it. Additionally, the effect of Mare Imbrium excavating the HPE reservoir on the interior temperature distribution is visible on the top left of Figure 4d.

Lastly, we note that the results of our laterally variable model setup remain consistent with the results of Laneuville et al. (2013, 2018) both in terms of average surface heat flux and mantle temperatures below the PKT region, which would allow for prolonged mare magmatism (∼3.5 Gyr) when compared to the solidus used in Laneuville et al. (2013). However, our setup does not explicitly model melting, and a reliable treatment of lunar magmatism would require considering a time-dependent solidus and processes such as mantle depletion, melt ascent and eruption, which is out of scope for this study. For this reason, we do not further discuss the implications of our modeling results on the volcanic history of the Moon.

4.3. Spatial Distribution of the Present-Day Surface Heat Flux on the Moon

Based on the results of Section 4.1, we exclude the cases of a globally uniform urKREEP layer and a complete remixing of urKREEP material into the mantle for the following analyses. Instead, we focus on regional and hemispherical HPE-unit cases, varying the bulk radiogenic concentration and anomaly enrichment for four HPE-rich unit geometries: ∼800 km (small), 1,200 km (medium), 1,600 km (large), and 2,700 km (hemispherical) in radius (Figure 5). Configurations that are consistent with both Apollo 15 and 17 results within 1-sigma level are deemed acceptable. Our modeled heat flux values at Region 5 (representative of the south polar region) are provided for context, but are not compared to the reported values in the literature as constraints, due to the absence of associated uncertainties. We note that care should also be taken when choosing the position of the center point for each HPE-rich unit scenario. More information on how this parameter was chosen in this study can be found in Supporting Information S1 (Section S2.2), along with plots showing surface heat flux distributions for each HPE-rich unit size scenario in Section S2.3 of the Supporting Information S1.

For a small HPE-rich unit (∼800 km), we find that no combination of bulk and HPE-rich unit enrichments produces heat flux values consistent with both Apollo measurements (Figure 5). This scenario is representative of all configurations in which Apollo 15 and 17 are both located outside of the anomaly. In addition, a similar crustal thickness underlies the two locations, implying that their heat flux is expected to be similar unless the HPE anomaly extends beneath one of the sites. In addition, fitting both Apollo values would require heat fluxes equal to 16–18 mW/m^2 outside of the anomaly, which implies unreasonably high bulk HPE concentrations (≥0.11 ppm Th), inconsistent with the range of 0.06–0.09 ppm Th provided by G. Taylor and Wieczorek (2014).

The medium unit case (∼1,200 km radius) represents all configurations in which Apollo 15 is located either within or at the edge of the anomaly, while Apollo 17 lies outside of it (e.g., Figure 4b, Apollo 15 on the unit edge). In this case, we find that a rather high bulk HPE concentration (∼0.09 ppm Th) and weak anomaly (∼30 ppm Th) are required to fit both Apollo measurements. High bulk concentrations are required to raise the

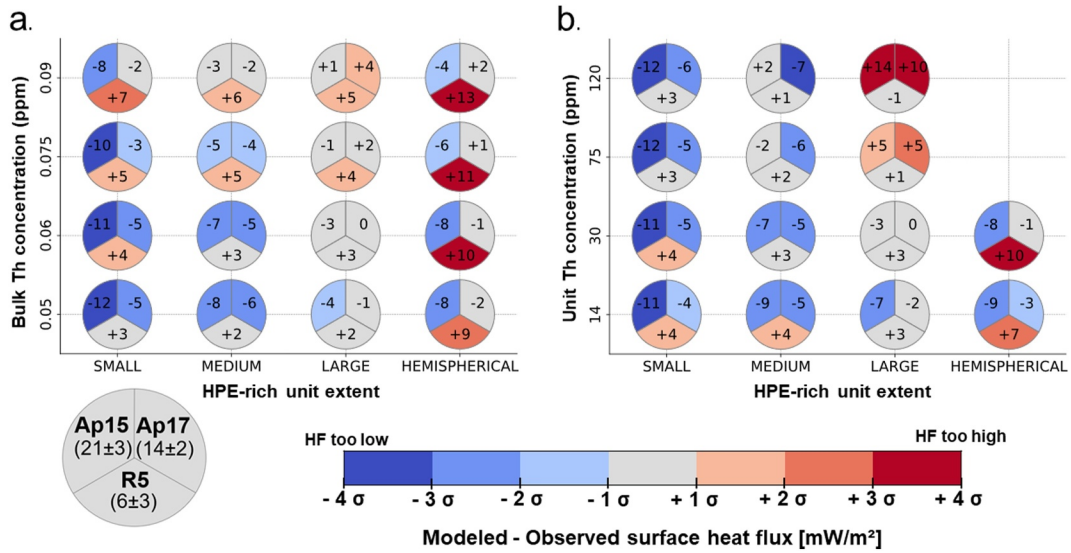

Figure 5. Summary of simulations varying the lateral extent of the HPE-rich unit versus the bulk (a) and the unit Th concentration (b). All models share a HPE-rich unit with an effective average thickness of 1.6 km. In panel (a) the HPE-rich unit has a Th concentration of 30 ppm, while in panel (b) the bulk concentration of Th is equal to ∼0.06 ppm. Each pie chart represents a separate simulation, and each pie chart sector a specific surface location: Apollo 15, Apollo 17, and Region 5. The fill color of each pie chart sector represents the difference between modeled and observed surface heat flux (i.e., Apollo 15: 21 mW/m^2, Apollo 17: 14 mW/m^2, and Region 5: 6 mW/m^2), with light blue/red pie charts corresponding to more realistic scenarios. Note: the error bar used for the Region 5 estimate (50%) has been chosen to represent a lower level of confidence in the value and allow for comparable visualization, but no uncertainty has been reported in the literature for this estimate. The absence of models in the right top corner of panel (b) is because these models would have a negative Th concentration in the mantle.

background heat flux to be consistent with Apollo 17 measurement, while values within the anomaly should not exceed Apollo 15 measurement, requiring a relatively weak asymmetry in Th concentrations.

For configurations with a large HPE-rich unit (∼1,600 km radius) we find most of our best-fit scenarios (Figure 5). In this configuration, Apollo 15 is representative of the center of the anomaly, while Apollo 17 is located on its edge. Under these conditions, bulk concentrations of 0.06–0.075 ppm Th and unit concentrations of 23–50 ppm Th are consistent with the measurements (end-member values are found through interpolation between models). In this case, bulk and unit concentrations are both low, causing the heat flux at the center of the anomaly to reach the Apollo 15 value, and values similar to Apollo 17 at its edge. In addition, this configuration is the only one that can also produce relatively low heat fluxes in the south polar region (8–9 mW/m^2), making the Region 5 heat flux estimate plausible only in a large HPE-rich unit configuration.

In case of a hemispherical HPE-rich unit (∼2,700 km radius), the anomaly is so large that it takes up most of the HPE available within the bulk Moon, leaving the mantle highly depleted. This case is a proxy for Apollo 15 and 17 being representative of a similar terrain in terms of HPE, both being located within the anomaly. Thus, we retrieve a similar heat flux values at the two locations. Contrary to the results of our simplified analysis, no parameter combination in Figure 5 can reach values as high as the original Apollo 15 measurement (21 mW/m^2). Reaching such high heat fluxes within a hemispherical unit would require high bulk and unit concentrations (>0.09 and 75 ppm Th, respectively). However, under this combination of parameters, Apollo 17 location would also display similar values, about 4 mW/m^2 too high.

We note that for all models in Figure 5a, increasing the bulk HPE abundances from 0.05 to 0.09 ppm Th (0.014–0.024 ppm U) corresponds to an increase of the average surface heat flux values from 10 to 13.5 mW/m^2, which is consistent with the results obtained in Warren and Rasmussen (1987), their Figure 8. Lastly, we note that exploring a broader parameter space with laterally variable crustal thickness and HPE-rich unit thickness offers several advantages over the models in Laneuville et al. (2013, 2018):

1. It allows us to rule out hemispherical and small-unit scenarios, as well as upper and lower end-member Th concentrations within the HPE anomaly, thereby narrowing down the parameter space.
2. It provides testable predictions of heat flux and thermal evolution beneath specific surface locations, providing valuable input for related fields such as geologic mapping, impact modeling, seismic inversions, and tidal response studies.
3. It mimics the effects of basin excavation and ejecta blanket deposition through the variable HPE-rich layer thickness.

5. Discussion

5.1. Geometrical Extent of the HPE Anomaly

The results presented in Section 4 can be summarized as follows:

1. Symmetric distributions of HPE in the Moon's interior are inconsistent with observations.
2. A nearside HPE anomaly should at least extend to beneath the Apollo 15 landing location.
3. Across all tested configurations, the anomaly is required to be rather weak (Th content ranging from 23 to 50 ppm for a 1.6 km thick layer, and proportionally lower for a thicker layer).
4. Bulk silicate Moon concentration of HPE can only be constrained as a function of the geographical extent of the anomaly, with the case of a medium anomaly favoring higher bulk HPE concentrations with respect to large anomaly scenarios.

In the following paragraphs, we will discuss the implications of our results on the current understanding of lunar structure and evolution.

Our results show that a globally uniform HPE-rich layer is inconsistent with Apollo measurements, and the nearside is required to be enriched in HPE with respect to the farside, assuming a range of 0.05–0.09 ppm bulk Th abundance (G. Taylor & Wieczorek, 2014). However, surface heat flow is only sensitive to the overall concentration of HPE beneath each surface location, and cannot disentangle different depth-wise distributions. This is why configurations with globally uniform layer or complete HPE remixing (Figures 3a and 3b, Section 4.1) produce similar surface heat flux distributions. Thus, our results cannot exclude the presence of some HPE-rich material underneath the entire crust, as suggested in Nagihara (2025), but require this HPE reservoir to be either thicker or more enriched underneath the nearside.

In our models, the HPE anomaly is required to extend at least beneath the landing site of Apollo 15, in order to explain its measured heat flux value. However, the observed heat flux difference between Apollo 15 and 17 has also been attributed to the effect of surface Th anomalies, which are thought to be Imbrium ejecta (Hagermann & Tanaka, 2006; Haskin, 1998). If this is the case, the HPE-rich anomaly could have been located only underneath Imbrium and excavated during its formation. This would allow the HPE-rich unit size to be similar to or smaller than our small anomaly scenario (Section S2.2 in Supporting Information S1). While these scenarios are plausible, they can only marginally reproduce the Apollo 15 heat flux value, as noted by Siegler and Smrekar (2014). In addition, cases where the HPE-unit is too small are more difficult to reconcile with the fact that the entire Oceanus Procellarum shows long-lasting volcanic activity, requiring sufficiently high subsurface temperatures to melt material over a period of ∼3 Gyr (Hiesinger et al., 2023).

Although we consider all models consistent with the Apollo measurements successful, the ability to locate surface features allows us to compare the extent of the HPE-rich unit with additional geophysical evidence. First, a HPE anomaly larger than 1,600 km in radius would extend beneath most nearside basins, which is inconsistent with the lack of strong Th signatures in the ejecta blankets from basins other than Imbrium. Among others, Mare Orientale is believed to be as young as Imbrium, and it is one of the regions of thinnest crust on the Moon, implying that the impact should have also excavated HPE-rich material. However, no strong Th signature can be seen surrounding Mare Orientale (Lawrence et al., 1999, 2003). A similar argument applies to Mare Serenitatis and Crisium, although their older age has been proposed to cause the dilution of their Th signatures through prolonged impact gardening during the late heavy bombardment (Nagihara, 2025).

The case of a HPE-rich unit extending up to the Apollo 17 location and eastern edge of Mare Serenitatis (1,500–1,600 km HPE-rich unit radius) appears more likely because its size corresponds to the nearside region of low crustal thickness (Figure 2) and thick mare basalt units (Broquet & Andrews-Hanna, 2024a). This configuration is

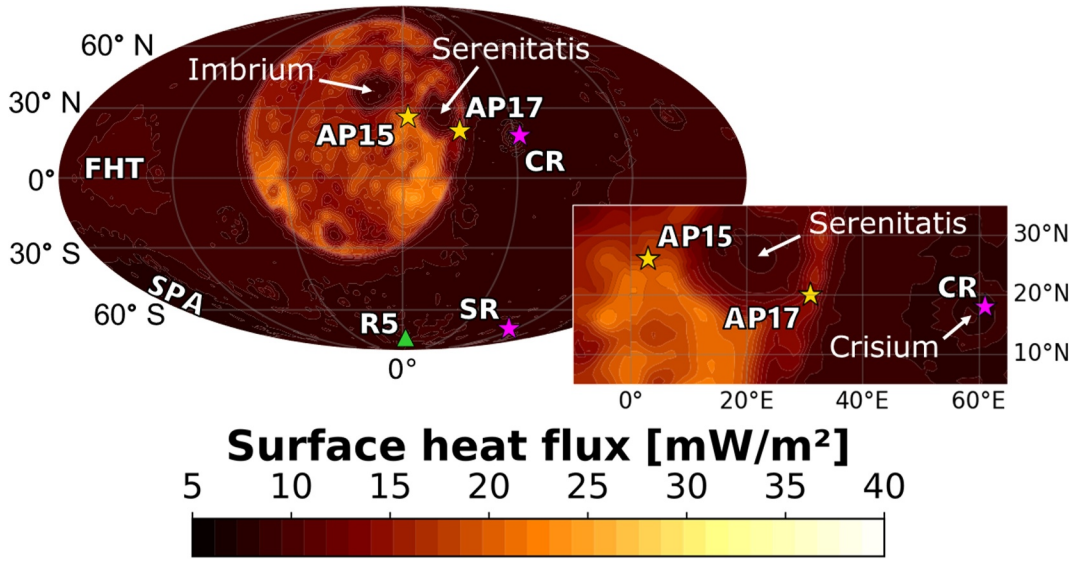

Figure 6. Surface heat flux map of our preferred large HPE-rich unit scenario (i.e., 1,600 km HPE-rich unit radius, 0.06 ppm bulk Th concentration, 0.4 ppm crustal Th concentration, 30 ppm HPE-rich unit Th concentration). The symbols in the map indicate the landing sites of Apollo 15 and Apollo 17 (AP15 and AP17), Region 5 (R5, south polar region), and future measurements locations (Mare Crisium—CR, Schrödinger Crater—SR). In addition, we indicate the Farside Highlands Terrane (FHT), South-Pole Aitken basin (SPA), Mare Imbrium, Serenitatis, and Crisium.

also the only scenario that produces a south polar heat flux lower than the Apollo 17 measurement. However, the lack of an Imbrium-like Th signature surrounding Mare Serenitatis remains partially unexplained in this scenario. The surface heat flux distribution for our preferred model with a large HPE-rich unit scenario is shown in Figure 6, including an enlarged inset of the region in the vicinity of Apollo 15, Apollo 17, and Blue Ghost-1 landing sites.

Alternatively, positioning the boundary of the HPE anomaly between the Apollo 15 and 17 landing sites or, in other words, having a HPE-rich unit that does not extend beneath Mare Serenitatis (medium unit in Section 4.3), could explain the missing Th signature. In this case, however, the heat flux at the south pole stays similar to that at the Apollo 17 location. A summary of present-day surface heat flux maps for all scenarios consistent with Apollo 15 and 17 heat flux constraints can be found in Supporting Information S1 (Section S2.4).

5.2. Origin of the Nearside HPE Anomaly

Assuming a range of 0.05–0.09 ppm bulk Th abundance (G. Taylor & Wieczorek, 2014), our modeling results require a HPE enrichment beneath the nearside, which implies that a process must have concentrated heat sources there during the Moon's evolution. However, the Apollo measurements are consistent with a relatively weak HPE asymmetry between the two hemispheres, independent of the lateral extent of the subsurface HPE-rich unit, suggesting a rather ineffective HPE redistribution process. Potential HPE redistribution processes have been proposed: (a) asymmetric LMO crystallization (Moriarty et al., 2021; Parmentier et al., 2002), (b) lateral transport of HPE triggered by a cataclysmic event, such as the South Pole–Aitken (SPA) impact (Jones et al., 2022; Zhang et al., 2022), (c) destablization and sinking of the urKREEP layer everywhere but underneath the PKT region (Liang et al., 2024).

In addition, we note that although our models cannot disentangle the HPE-rich unit thickness and radiogenic enrichment, investigating the timing of HPE sequestration underneath the PKT can help us to independently constrain these two key parameters. If the HPE redistribution process occurs during the LMO crystallization, the resulting HPE-rich unit can become more enriched than what is predicted by 1D LMO crystallization models, for instance due to the lateral migration of incompatible elements. Conversely, if the HPE redistribution happens through solid-state convection, after the complete crystallization of the LMO, the concentration of HPE in the resulting unit should be similar to that of a global layer, but its thickness can vary.

5.3. Model Limitations

The high local heat flux estimate at the Compton-Belkovich region (180 mW/m^2, Siegler et al., 2023) is challenging to capture using a global model. None of our scenarios is able to produce a high surface heat flux anomaly at the Compton-Belkovich region. Compton-Belkovich is characterized by an average crustal thickness value for the nearside (∼32 km), and we do not prescribe any local HPE anomaly in the region, which means that in our setup there is no reason for a heat flux enhancement there.

Reprocessing of surface Th concentration data confirms the presence of a high Th abundance (40–55 ppm) in a region of 30–60 km in diameter at Compton-Belkovich (Lawrence et al., 2003). The high surface heat flux is suggested to be the result of a subsurface pluton of evolved granitic composition with respect to typical KREEP basalt (Siegler et al., 2023). The Th concentration proposed for the magmatic intrusion ranges between ∼60–-130 ppm, depending on the volume of intruded material, and is confined in a region of just a few tens of kilometers in diameter. Considering that this diameter is comparable to the lateral resolution of our model at the surface (∼30 km), a regional model is needed to investigate small-scale Th anomalies such as Compton-Belkovich.

We do not consider mantle melting, impacts, or tidal dissipation in our modeled energy balance within the Moon. Although these processes are thought to affect the interior temperature distribution during the evolution, they mostly played an important role during the earliest stages of lunar evolution. Indeed, magmatic activity experienced a primary peak between 3.2 and 3.6 Ga, and a secondary peak around 2 Ga, with very little melt being extruded afterward (Hiesinger et al., 2023, and references therein). Major impacts, capable of substantially affecting the thermal history of the Moon, ceased to occur after the late heavy bombardment around 3.8 Ga, and the energy input from tidal dissipation only dominates during the first 10^4 years of lunar evolution (Andrews-Hanna et al., 2023). Since we focus on the present-day thermal state of the Moon, such processes have been neglected in our study. However, mantle melting, impacts, and tides should be included in future thermal evolution studies to investigate their effects on the early stages of the lunar history.

Finally, our models employ a chemically homogeneous mantle, which is known to be a strong assumption for thermal evolution modeling (Andrews-Hanna et al., 2023). An initially layered mantle, resulting from the solidification of the LMO, could affect the vigor of convection throughout the evolution. However, modeling the effects of an initially layered lunar mantle on the thermal history of the Moon requires a careful coupling with LMO crystallization models, similar to those in Schwinger and Breuer (2022), and computationally costly composition tracking (Bernt et al., 2024) which is beyond the scope of this study.

5.4. Implications for Future Heat Flux Measurement Sites

Due to the limited number of in situ measurements of surface heat flux on the Moon, and the uncertainties of remote sensing-based estimates, obtaining new data is crucial to further constrain the HPE distribution in the lunar interior. Even one additional in-situ measurement would greatly improve our models of the lunar thermal state, if conducted at a well chosen site. In particular, any new measurement taken outside of the PKT surface Th anomaly would allow us to place tighter constraints on the average surface heat flux and its lateral variations, using thermal evolution models similar to those presented in this work.

In turn, the average surface heat flux provides a constraint on the Moon's bulk HPE abundance via the Urey ratio (ratio of internal heat production to surface heat loss) as was proposed for Mars (Plesa et al., 2015). Across all our model configurations, we find a present-day Urey ratio of ∼0.8, independent of the model parameters. Combined with a robust estimate of the average heat flux of the Moon, our models could further constrain the heat production rate of the lunar interior and with it the composition of the primordial Moon.

Second, measuring surface heat flux in regions far from high-Th anomalies, such as Mare Crisium (Blue Ghost-1 landing site) or Schrödinger Crater (future landing site of APEX®1.0 mission by ispace-U.S.) can provide new direct constraints on the lateral extent and enrichment of the nearside HPE anomaly (see Section 5.1). In addition, taking measurements in regions likely to exhibit heat flux maxima, such as Aristarchus Plateau, would also help to establish crucial upper bounds on the lunar surface heat flux.

Our models can provide local predictions of the surface heat flux anywhere on the Moon at any given time, including the locations where future heat flux measurements will be performed, such as Mare Crisium and Schrödinger crater. Thus, our best-fit models offer a valuable baseline for interpreting future heat flux data. Based

on the surface heat flux distribution of models consistent with Apollo data (Section 4.3), we find heat flux ranges of 7–12 mW/m^2 and 8–14 mW/m^2 for the Mare Crisium and Schrödinger Crater locations, respectively. Any substantial difference to such values could indicate a more complex HPE distribution in the interior of the Moon, which can be readily tested using our setup.

Finally, we propose the Aristarchus Plateau on the nearside and the feldspathic highlands terrain (FHT in Figure 4) on the farside as key landing sites for future heat flow probes. Aristarchus Plateau is characterized by the most recent volcanic flows on the Moon (Hiesinger et al., 2023), and could provide insights into the HPE concentration most representative of the center of the nearside thermal anomaly (Laneuville et al., 2013). Conversely, the feldspathic highlands terrain on the farside could provide heat flux data at the region of thickest crust on the Moon, helping to constrain bulk HPE concentrations in the lunar crust and reduce the current nearside bias in heat flux measurements.

6. Conclusions

In this study, we employed a 3D global geodynamic model to investigate the thermal evolution of the Moon and its interior structure. Our model setup builds on previous work (Laneuville et al., 2013, 2018) by incorporating lateral variations in crustal thickness and a more complex geometry for the HPE-rich unit. Additionally, we conducted a parameter exploration guided by recent constraints on the composition and structure of the lunar interior (Haupt et al., 2024; Levin et al., 2025; Schwinger & Breuer, 2022). Best-fit scenarios were selected based on surface heat flux measurements at the Apollo 15 and 17 landing sites, and subsequently compared with recent heat flux estimates (Paige & Siegler, 2016; Wei et al., 2023) and geological evidence such as age and distribution of mare basalt units (Hiesinger et al., 2023), and surface Th distribution (Lawrence et al., 2003).

Our results indicate that a globally uniform HPE-rich layer beneath the crust or fully mixed within the mantle (i.e., global overturn) is inconsistent with the Apollo heat flow data. Instead, our findings support the presence of a HPE anomaly beneath the nearside, assuming ±20% bulk silicate Earth Th abundance (G. Taylor & Wieczorek, 2014). The HPE anomaly is constrained to extend at least from Aristarchus Plateau to the Apollo 15 landing site (∼1,200 km in radius), and in the largest scenario, extending beneath most of the nearside hemisphere (>1,600 km). Furthermore, the HPE concentrations in the anomaly is required to be in the range of 23–50 ppm Th, for a 1.6 km-thick unit, with proportionally lower concentrations for a thicker layer. These results suggest that some process sequestered radiogenics beneath the lunar nearside, but it was likely an inefficient process.

Finally, our models predict heat flux ranges of 7–12 mW/m^2 for the measurement planned by Firefly's Blue Ghost Mission 1 at Mare Crisium, and 8–14 mW/m^2 for Ispace's APEX®1.0 at Schrödinger Crater. Each new heat flux measurement will provide a key constraint on the subsurface distribution of HPE and greatly improve our understanding of the Moon's asymmetrical thermal evolution. Based on our results, we propose Aristarchus Plateau and the Farside Highlands Terrane (FHT) as regions of interest for future heat flux experiments.

Conflict of Interest

The authors declare no conflicts of interest relevant to this study.

Data Availability Statement

All data presented in this paper, along with supplementary data sets for all models are available in Supporting Information S1 and in tabulated form on Zenodo (Santangelo et al., 2025). The GAIA code is a proprietary code of DLR. Users interested in working with it should contact Ana-Catalina Plesa (ana.plesa@dlr.de) and Christian Hüttig (christian.huettig@dlr.de).

Acknowledgments
We thank Matt J. Jones and Seiichi Nagihara for comments that helped improve the manuscript, and Jean-Pierre Williams for his editorial work. SS and ACP acknowledge funding from the Deutsche Forschungsgemeinschaft (DFG, German Research Foundation)—Project-ID 551620924. AB is funded by the Alexander von Humboldt Foundation. The authors gratefully acknowledge the scientific support and HPC resources provided by the German Aerospace Center (DLR). The HPC system CARA is partially funded by "Saxon State Ministry for Economic Affairs, Labor and Transport" and "Federal Ministry for Economic Affairs and Climate Action." The HPC system CARO is partially funded by "Ministry of Science and Culture of Lower Saxony" and "Federal Ministry for Economic Affairs and Climate Action." Open Access funding enabled and organized by Projekt DEAL.

References

Andrews-Hanna, J. C., Weber, R. C., Garrick-Bethell, I., Evans, A. J., Kiefer, W. S., Grimm, R. E., et al. (2023). The structure and evolution of the lunar interior. *Reviews in Mineralogy and Geochemistry*, *89*(1), 243–292. https://doi.org/10.2138/rmg.2023.89.06

Bernt, I., Schwinger, S., Plesa, A.-C., & Breuer, D. (2024). Moons crust evolution: Combining petrological with geodynamical models. In *Europlanet science congress* (p. EPSC2024-1242). https://doi.org/10.5194/epsc2024-1242

Broquet, A., & Andrews-Hanna, J. (2024a). The moon before mare. *Icarus*, *408*, 115846. https://doi.org/10.1016/j.icarus.2023.115846

Broquet, A., & Andrews-Hanna, J. (2024b). A volcanic inventory of the Moon. *Icarus*, *411*, 115954. https://doi.org/10.1016/j.icarus.2024.115954
Gaffney, A. M., Gross, J., Borg, L. E., Hanna, K. L. D., Draper, D. S., Dygert, N., et al. (2023). Magmatic evolution I: Initial differentiation of the Moon. *Reviews in Mineralogy and Geochemistry*, *89*(1), 103–145. https://doi.org/10.2138/rmg.2023.89.03
Grott, M., Knollenberg, J., & Krause, C. (2010). Apollo lunar heat flow experiment revisited: A critical reassessment of the in situ thermal conductivity determination. *Journal of Geophysical Research*, *115*(E11), E11005. https://doi.org/10.1029/2010je003612
Hagermann, A., & Tanaka, S. (2006). Ejecta deposit thickness, heat flow, and a critical ambiguity on the Moon. *Geophysical Research Letters*, *33*(19), L19203. https://doi.org/10.1029/2006gl027030
Haskin, L. A. (1998). The imbrium impact event and the thorium distribution at the lunar highlands surface. *Journal of Geophysical Research*, *103*(E1), 1679–1689. https://doi.org/10.1029/97je03035
Haupt, C. P., Renggli, C. J., Rohrbach, A., Berndt, J., Schwinger, S., Maurice, M., et al. (2024). Trace element partitioning in the lunar magma ocean: An experimental study. *Contributions to Mineralogy and Petrology*, *179*(5), 45. https://doi.org/10.1007/s00410-024-02118-z
Hiesinger, H., van der Bogert, C., Michael, G., Schmedemann, N., Iqbal, W., Robbins, S., et al. (2023). The lunar cratering chronology. *Reviews in Mineralogy and Geochemistry*, *89*(1), 401–451. https://doi.org/10.2138/rmg.2023.89.10
Hüttig, C., & Stemmer, K. (2008a). Finite volume discretization for dynamic viscosities on voronoi grids. *Physics of the Earth and Planetary Interiors*, *171*(1–4), 137–146. https://doi.org/10.1016/j.pepi.2008.07.007
Hüttig, C., & Stemmer, K. (2008b). The spiral grid: A new approach to discretize the sphere and its application to mantle convection. *Geochemistry, Geophysics, Geosystems*, *9*(2), Q02018. https://doi.org/10.1029/2007gc001581
Hüttig, C., Tosi, N., & Moore, W. B. (2013). An improved formulation of the incompressible Navier–Stokes equations with variable viscosity. *Physics of the Earth and Planetary Interiors*, *220*, 11–18. https://doi.org/10.1016/j.pepi.2013.04.002
Jolliff, B. L., Gillis, J. J., Haskin, L. A., Korotev, R. L., & Wieczorek, M. A. (2000). Major lunar crustal terranes: Surface expressions and crust-mantle origins. *Journal of Geophysical Research*, *105*(E2), 4197–4216. https://doi.org/10.1029/1999je001103
Jones, M. J., Evans, A. J., Johnson, B. C., Weller, M. B., Andrews-Hanna, J. C., Tikoo, S. M., & Keane, J. T. (2022). A South Pole–Aitken impact origin of the lunar compositional asymmetry. *Science Advances*, *8*(14), eabm8475. https://doi.org/10.1126/sciadv.abm8475
Karato, S.-I., & Wu, P. (1993). Rheology of the upper mantle: A synthesis. *Science*, *260*(5109), 771–778. https://doi.org/10.1126/science.260.5109.771
Laneuville, M., Taylor, G. J., & Wieczorek, M. A. (2018). Distribution of radioactive heat sources and thermal history of the Moon. *Journal of Geophysical Research: Planets*, *123*(12), 3144–3166. https://doi.org/10.1029/2018je005742
Laneuville, M., Wieczorek, M. A., Breuer, D., & Tosi, N. (2013). Asymmetric thermal evolution of the Moon. *Journal of Geophysical Research: Planets*, *118*(7), 1435–1452. https://doi.org/10.1002/jgre.20103
Langseth, M. G., Keihm, S. J., & Peters, K. A. (1976). The revised lunar heat flow values. Retrieved from https://api.semanticscholar.org/CorpusID:91317287
Lawrence, D. J., Elphic, R. C., Feldman, W. C., Prettyman, T. H., Gasnault, O., & Maurice, S. (2003). Small-area thorium features on the lunar surface. *Journal of Geophysical Research*, *108*(E9), 5102. https://doi.org/10.1029/2003je002050
Lawrence, D. J., Feldman, W. C., Barraclough, B. L., Binder, A. B., Elphic, R. C., Maurice, S., et al. (1999). High resolution measurements of absolute thorium abundances on the lunar surface. *Geophysical Research Letters*, *26*(17), 2681–2684. https://doi.org/10.1029/1999gl008361
Levin, J. N., Evans, A. J., Andrews-Hanna, J. C., & Daubar, I. J. (2025). Lunar crustal KREEP distribution. *Journal of Geophysical Research: Planets*, *130*(1), e2024JE008418. https://doi.org/10.1029/2024je008418
Liang, W., Broquet, A., Andrews-Hanna, J. C., Zhang, N., Ding, M., & Evans, A. J. (2024). Vestiges of a lunar ilmenite layer following mantle overturn revealed by gravity data. *Nature Geoscience*, *17*(4), 361–366. https://doi.org/10.1038/s41561-024-01408-2
Longhi, J. (1980). A model of early lunar differentiation. In *Lunar and planetary science conference, 11th, Houston, TX, March 17–21, 1980, proceedings. Volume 1. (a82-22251 09-91) New York* (Vol. 11, pp. 289–315). Pergamon Press.
Meyer, C. (2004). Lunar sample compendium. NASA STI/Recon Technical Report N, 6, 11039.
Moriarty, D. P., Dygert, N., Valencia, S. N., Watkins, R. N., & Petro, N. E. (2021). The search for lunar mantle rocks exposed on the surface of the Moon. *Nature Communications*, *12*(1), 4659. https://doi.org/10.1038/s41467-021-24626-3
Nagihara, S. (2025). A global survey of lunar surface thorium anomalies associated with impact basins. *The Planetary Science Journal*, *6*(2), 30. https://doi.org/10.3847/psj/ada49e
Paige, D., & Siegler, M. (2016). New constraints on lunar heat flow rates from LRO diviner lunar radiometer experiment polar observations. (47th ed.).
Parmentier, E., Zhong, S., & Zuber, M. (2002). Gravitational differentiation due to initial chemical stratification: Origin of lunar asymmetry by the creep of dense KREEP? *Earth and Planetary Science Letters*, *201*(3–4), 473–480. https://doi.org/10.1016/s0012-821x(02)00726-4
Plesa, A.-C., Grott, M., Tosi, N., Breuer, D., Spohn, T., & Wieczorek, M. A. (2016). How large are present-day heat flux variations across the surface of Mars? Mars heat flux. *Journal of Geophysical Research: Planets*, *121*(12), 2386–2403. https://doi.org/10.1002/2016je005126
Plesa, A.-C., Hüttig, C., Maurice, M., Breuer, D., & Tosi, N. (2016). Large scale numerical simulations of planetary interiors (pp. 675–687).
Plesa, A.-C., Tosi, N., Grott, M., & Breuer, D. (2015). Thermal evolution and urey ratio of Mars: Mars Urey ratio. *Journal of Geophysical Research: Planets*, *120*(5), 995–1010. https://doi.org/10.1002/2014je004748
Santangelo, S., Plesa, A.-C., Broquet, A., Breuer, D., & Grott, M. (2025). Present-day thermal state and surface heat flux of the Moon [Dataset]. *Zenodo*. https://doi.org/10.5281/zenodo.17162838
Schubert, G., Cassen, P., & Young, R. (1979). Subsolidus convective cooling histories of terrestrial planets. *Icarus*, *38*(2), 192–211. https://doi.org/10.1016/0019-1035(79)90178-7
Schwinger, S., & Breuer, D. (2022). Employing magma ocean crystallization models to constrain structure and composition of the lunar interior. *Physics of the Earth and Planetary Interiors*, *322*, 106831. https://doi.org/10.1016/j.pepi.2021.106831
Siegler, M., Feng, J., Lehman-Franco, K., Andrews-Hanna, J. C., Economos, R. C., Clair, M. S., et al. (2023). Remote detection of a lunar granitic batholith at Compton–Belkovich. *Nature*, *620*(7972), 116–121. https://doi.org/10.1038/s41586-023-06183-5
Siegler, M., & Smrekar, S. (2014). Lunar heat flow: Regional prospective of the Apollo landing sites. *Journal of Geophysical Research: Planets*, *119*(1), 47–63. https://doi.org/10.1002/2013je004453
Smith, D. E., Zuber, M. T., Neumann, G. A., Lemoine, F. G., Mazarico, E., Torrence, M. H., et al. (2010). Initial observations from the lunar orbiter laser altimeter (LOLA). *Geophysical Research Letters*, *37*(18), L18204. https://doi.org/10.1029/2010gl043751
Steinbach, V., & Yuen, D. A. (1994). Effects of depth-dependent properties on the thermal anomalies produced in flush instabilities from phase transitions. *Physics of the Earth and Planetary Interiors*, *86*(1–3), 165–183. https://doi.org/10.1016/0031-9201(94)05067-8
Stevenson, D. J., Spohn, T., & Schubert, G. (1983). Magnetism and thermal evolution of the terrestrial planets. *Icarus*, *54*(3), 466–489. https://doi.org/10.1016/0019-1035(83)90241-5

Taylor, G., & Wieczorek, M. (2014). Lunar bulk chemical composition: A post-gravity recovery and interior laboratory reassessment. *Philosophical Transactions of the Royal Society A: Mathematical, Physical and Engineering Sciences*, *372*(2024), 20130242. https://doi.org/10.1098/rsta.2013.0242

Taylor, S. (1982). *Planetary science: A lunar perspective* (1th ed.). 3303 NASA ROAD 1, Lunar and Planetary Institute.

Warren, P. H., & Rasmussen, K. L. (1987). Megaregolith insulation, internal temperatures, and bulk uranium content of the Moon. *Journal of Geophysical Research*, *92*(B5), 3453–3465. https://doi.org/10.1029/jb092ib05p03453

Warren, P. H., & Wasson, J. T. (1979). The origin of KREEP. *Reviews of Geophysics*, *17*(1), 73–88. https://doi.org/10.1029/rg017i001p00073

Wei, G., Li, X., Gan, H., & Shi, Y. (2023). Retrieval of lunar polar heat flow from Chang'E-2 microwave radiometer and diviner observations. *Frontiers in Astronomy and Space Sciences*, *10*, 1179558. https://doi.org/10.3389/fspas.2023.1179558

Wieczorek, M. A., Neumann, G. A., Nimmo, F., Kiefer, W. S., Taylor, G. J., Melosh, H. J., et al. (2013). The crust of the Moon as seen by grail. *Science*, *339*(6120), 671–675. https://doi.org/10.1126/science.1231530

Wieczorek, M. A., & Phillips, R. J. (2000). The "Procellarum KREEP Terrane": Implications for mare volcanism and lunar evolution. *Journal of Geophysical Research*, *105*(E8), 20417–20430. https://doi.org/10.1029/1999je001092

Zhang, Ding, M., Zhu, M.-H., Li, H., Li, H., & Yue, Z. (2022). Lunar compositional asymmetry explained by mantle overturn following the South Pole–Aitken impact. *Nature Geoscience*, *15*(1), 37–41. https://doi.org/10.1038/s41561-021-00872-4

Zuber, M. T., Smith, D. E., Watkins, M. M., Asmar, S. W., Konopliv, A. S., Lemoine, F. G., et al. (2013). Gravity field of the Moon from the Gravity Recovery and Interior Laboratory (GRAIL) mission. *Science*, *339*(6120), 668–671. https://doi.org/10.1126/science.1231507

References From the Supporting Information

Beattie, P., Ford, C., & Russel, D. (1993). Partition coefficients for olivine-melt and orthopyroxene-melt systems. *Contributions to Mineralogy and Petrology*, *114*(2), 288. https://doi.org/10.1007/bf00307763

Kelemen, P. B., Shimizu, N., & Dunn, T. (1993). Relative depletion of niobium in some arc magmas and the continental crust: Partitioning of K, Nb, La and Ce during melt/rock reaction in the upper mantle. *Earth and Planetary Science Letters*, *120*(3–4), 111–134. https://doi.org/10.1016/0012-821x(93)90234-z

McKENZIE, D., & O'Nions, R. K. (1991). Partial melt distributions from inversion of rare Earth element concentrations. *Journal of Petrology*, *32*(5), 1021–1091. https://doi.org/10.1093/petrology/32.5.1021

Onuma, N., Higuchi, H., Wakita, H., & Nagasawa, H. (1968). Trace element partition between two pyroxenes and the host lava. *Earth and Planetary Science Letters*, *5*, 47–51. https://doi.org/10.1016/s0012-821x(68)80010-x

Roberts, J. H., & Zhong, S. (2006). Degree-1 convection in the Martian mantle and the origin of the hemispheric dichotomy. *Journal of Geophysical Research*, *111*(E6), E06013. https://doi.org/10.1029/2005je002668

Roy, A., Mallik, A., Bremner, P., Diamond, M. R., Haviland, H. F., Hervig, R. L., & Goepfert, T. J. (2024). How hot is the Moon: Quantifying the role of heat-producing elements on the present-day selenotherm with partitioning experiments and conductive thermal modeling. https://doi.org/10.22541/au.171753137.70879030/v1

Salters, V. J., & Longhi, J. (1999). Trace element partitioning during the initial stages of melting beneath mid-ocean ridges. *Earth and Planetary Science Letters*, *166*(1–2), 15–30. https://doi.org/10.1016/s0012-821x(98)00271-4

Schnetzler, C., & Philpotts, J. A. (1970). Partition coefficients of rare-earth elements between igneous matrix material and rock-forming mineral phenocrysts—II. *Geochimica et Cosmochimica Acta*, *34*(3), 331–340. https://doi.org/10.1016/0016-7037(70)90110-9

Schubert, G., Turcotte, D. L., & Olson, P. (2001). *Mantle convection in the Earth and planets*. Cambridge University Press.